Article ID: 1000-7032(2021)09-1396-07

Temperature-dependent Photoluminescence Properties of $Cs_{0.05}FA_{0.79}MA_{0.16}PbI_{2.52}Br_{0.48}$ Perovskite Thin Film

ZHANG Qiong, WU Yue-jia, FENG Yan-qin, SUN Li-wei, DAI Jun*

(*School of Science, Jiangsu University of Science and Technology, Zhenjiang* 212100, *China*)

* *Corresponding Author, E-mail: daijun@just.edu.cn*

Abstract: This paper reports the temperature-dependent photoluminescence properties of $Cs_{0.05}FA_{0.79}MA_{0.16}PbI_{2.52}Br_{0.48}$ perovskite thin film. The $Cs_{0.05}FA_{0.79}MA_{0.16}PbI_{2.52}Br_{0.48}$ perovskite thin film was prepared by one-step spin coating with chlorobenzene anti-solvent treatment, and the surface morphology and crystallization quality were characterized. The X-ray diffraction(XRD) indicates that the $Cs_{0.05}FA_{0.79}MA_{0.16}PbI_{2.52}Br_{0.48}$ has a typical tetragonal perovskite structure. The perovskite film has a uniform and dense surface, and the grain size is about 300 nm. The photoluminescence intensity was measured in the temperature range of 5 – 200 K. The photoluminescence spectra show a continuous blue shift of about 9.36 nm, and there is no reversal redshift induced by phase transition. The photoluminescence intensity shows a bi-exponential quenching with the increase of temperature, and two thermal activation energies are obtained by Arrhenius equation. The optical bandgap is fitted by the Bose-Einstein double harmonic oscillator model, and the non-renormalized bandgap energy, the energies of acoustic phonon and optical phonon were fitted. The photoluminescence broadening mechanism was studied by the Segall formula. At 10 K and 100 K, the photoluminescence is mainly from exciton recombination, while at 200 K, the radiation recombination is mainly from free-to-bound and donor-acceptor pairs, which means the defect associated photoluminescence arises at high temperature. The detailed optical parameters in our paper can provide a physical foundation for further optimization of perovskite optoelectronic devices.

Key words: perovskite thin film; photoluminescence; exciton-phonon interaction

CLC number: O482.31 **Document code**: A **DOI**: 10.37188/CJL.20210195

$Cs_{0.05}FA_{0.79}MA_{0.16}PbI_{2.52}Br_{0.48}$ 钙钛矿薄膜的变温光致发光特性

张 琼, 吴悦嘉, 冯艳琴, 孙立伟, 戴 俊*

(江苏科技大学 理学院, 江苏 镇江 212100)

摘要: 报道了 $Cs_{0.05}FA_{0.79}MA_{0.16}PbI_{2.52}Br_{0.48}$ 钙钛矿薄膜的变温光致发光特性。采用一步旋涂法,用氯苯作反溶剂制备了 $Cs_{0.05}FA_{0.79}MA_{0.16}PbI_{2.52}Br_{0.48}$ 钙钛矿薄膜,并对其表面形貌和结晶质量进行了表征。X 射线衍射(XRD)分析结果表明其为四方钙钛矿结构。钙钛矿薄膜表面均匀致密,晶粒尺寸约为 300 nm。在 5 ~ 200 K 温度范围内测量了光致发光强度,结果表明,光致发光光谱连续蓝移约 9.36 nm,没有相变引起的反转红移。光致发光强度随温度的升高呈双指数降低,由 Arrhenius 方程拟合得到了两个热激活能。通过玻色-爱因斯坦双谐振子模型对光学带隙进行了拟合,并对非重整化带隙能量、声学声子能量和光学声子能量也进行了拟

收稿日期: 2021-05-25; **修订日期**: 2021-07-06
基金项目: 国家自然科学基金(11874185)资助项目
Supported by National Natural Science Foundation of China(11874185)

合。通过 Segall 公式拟合光致发光的半峰宽(FWHM),研究了激子-声子相互作用对光致发光展宽的影响。在 10 K 和 100 K 时,光致发光主要来自激子复合;而在 200 K 时,辐射复合主要来自自由-束缚对和施主-受主对,这意味着缺陷相关的光致发光是在高温下产生的。本文详细的光学参数可以为钙钛矿型光电器件的研究提供物理基础。

关　键　词: 钙钛矿薄膜; 变温光致发光; 激子-声子相互作用

1　Introduction

In recent years, with the significant improvement of the performance of organic-inorganic metal halide perovskite solar cells, perovskite semiconductor was regarded as the ideal photovoltaic material to substitute the traditional silicon. Meanwhile, perovskite semiconductor materials also present excellent advantages in the light-emitting diodes, lasers and photodetectors. Therefore, semiconductor perovskite materials attract tremendous attention in the field of optoelectronics. The performance of optoelectronics devices strongly depends on the basic properties of carriers, such as the exciton binding energy, diffusion length, carrier-phonon interaction, and so on. Except for the organic-inorganic halide perovskite $MAPbX_3$[1-2] and pure inorganic perovskite $CsPbX_3$[3-4], scientists found many kinds of multiple cation perovskite $CsFAMAPbI_3$[5] can present higher power conversion efficiency than the $MAPbI_3$ and $CsPbI_3$ perovskite solar cell[6-9], so the $CsFAMAPbI_3$ is widely accepted as the active layer for the solar cell, and the $Cs_{0.05}(FA_{0.83}MA_{0.17})_{0.95}Pb(I_{0.83}Br_{0.17})_3$ achieves the best efficiency of 20.48%[10]. Usually, the $MAPbI_3$ perovskite bandgap changes with temperature, and phase transition can take place at about 120 K[11-13], which leads to the photoluminescence center reversal redshift. However, the temperature-dependent bandgap, photoluminescence profile and the carrier-phonon interaction have not been studied for such mixed cation perovskite $CsFAMAPb(I/Br)_3$.

In this paper, the optical properties of the $Cs_{0.05}FA_{0.79}MA_{0.16}PbI_{2.52}Br_{0.48}$ perovskite thin film with the reported highest power conversion efficiency was investigated. The $Cs_{0.05}FA_{0.79}MA_{0.16}PbI_{2.52}Br_{0.48}$ thin film was fabricated by spin-coating method, and the X-ray diffraction(XRD) and field-emission scanning electron microscope(FE-SEM) were measured to characterize the structure. The temperature-dependent photoluminescence center wavelength presents continuous blueshift as the temperature changes from 5 K to 200 K. The photoluminescence linewidth presents broadening as the temperature increases. The exciton binding energy, non-renormalization bandgap energy, electron-phonon coupling coefficient, optical and acoustic phonon energy are systematically studied.

2　Experiments

Formamidinium iodide(FAI) and methylammonium bromide(MABr) were bought from Dyesol. Lead iodide(PbI_2) and lead bromide($PbBr_2$) were bought from Sigma-Aldrich. Cesium iodide(CsI) was bought from Alfa Aesar. The perovskite precursor solutions were prepared by dissolving CsI(0.057 mol·L^{-1}), FAI(1.16 mol·L^{-1}), PbI_2(1.24 mol·L^{-1}), MABr(0.23 mol·L^{-1}) and $PbBr_2$(0.238 mol·L^{-1}) in the mixed solvent of DMF∶DMSO = 4∶1(volume ratio). The solution was stirred at 60 ℃ for 10 h and then filtered through a polytetrafluoroethylene filter(pore diameter 0.22 μm).

Indium-tin oxide glass substrates were sonicated for 15 min with detergent, deionized water, acetone and anhydrous ethanol, respectively. The substrates are dried by nitrogen, then cleaned in the UV-ozone cleaner for 15 min. The cleaned substrates were transferred to a nitrogen glove box. The perovskite precursor solution was spin-coated on ITO substrates with 6 000 r/min for 30 s in a nitrogen glove box, at the 20 th second, dip 200 μL chlorobenzene quickly to improve the perovskite crystalline quality. Then the obtained $Cs_{0.05}FA_{0.79}MA_{0.16}PbI_{2.52}Br_{0.48}$ perovskite thin film was annealed at 100 ℃ on the heating

plate for 30 min.

Under the irradiation of Cu Kα (λ = 0.154 056 nm), XRD of the $Cs_{0.05}FA_{0.79}$-$MA_{0.16}PbI_{2.52}Br_{0.48}$ thin film was measured by Bruker D8 superior diffractometer, and the morphology of the sample was measured by scanning electron microscope (Zeiss SURRA-40). The sample was positioned in a quartz optical cavity, refrigerated to 5 K through liquid nitrogen cryogenic system (Janis 150c), excited by means of 325 nm laser, then temperature was adjusted from 5 K to 200 K, and the photoluminescence spectra was amassed by means of a spectrometer geared up with CCD(SP 2500i, Acton).

3 Results and Discussion

Fig. 1(a) shows SEM image of $Cs_{0.05}FA_{0.79}$-$MA_{0.16}PbI_{2.52}Br_{0.48}$ perovskite thin film and the scale bar is 3 μm. The complete film is composed of uniform and dense perovskite layer, and the grain size is about 300 nm.

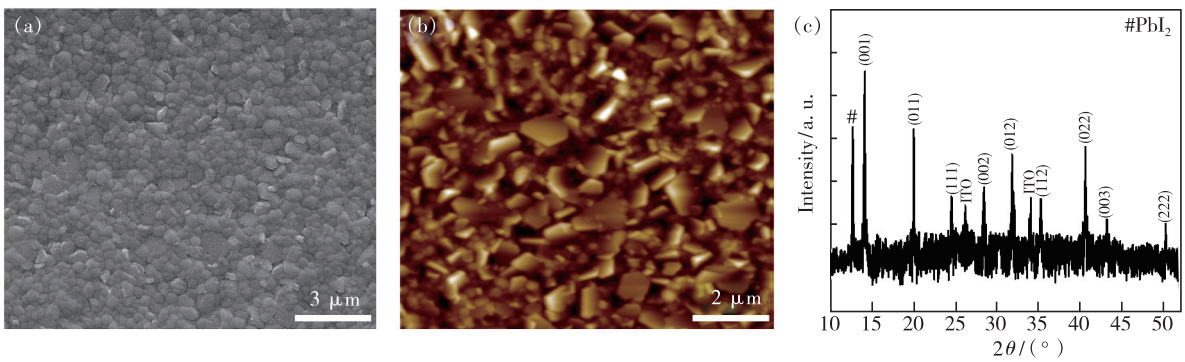

Fig. 1 SEM image(a), AFM image(b) and XRD pattern(c) of $Cs_{0.05}FA_{0.79}MA_{0.16}PbI_{2.52}Br_{0.48}$ perovskite thin film.

Fig. 1(b) shows the AFM image of as-fabricated film with the root mean square roughness of 36.9 nm. Fig. 1(c) shows the XRD pattern of $Cs_{0.05}$-$FA_{0.79}MA_{0.16}PbI_{2.52}Br_{0.48}$ perovskite thin film coated on ITO substrates. In the X-ray diffraction pattern, except for the diffraction from the ITO substrate and PbI_2, the other Bragg signals can be assigned to tetragonal perovskite phases. The obvious peak at 12.73° indicates that there is excess lead iodide (PbI_2) in the solutions of $Cs_{0.05}FA_{0.79}MA_{0.16}PbI_{2.52}$-$Br_{0.48}$ precursor and the peaks at 14.16°, 20.06°, 24.61°, 28.49°, 31.88°, 35.33°, 40.68°, 43.2° and 50.31° can be assigned to the scattering from (001), (011), (111), (002), (012), (112), (022), (003) and (222) crystal plane of the layered perovskite[14-17]. The signals of 14.16°, 20.06° and 24.61°(2θ Cu radiation) were observed from the X-ray diffraction patterns. The PbI_2 signal is widely presented in the perovskite samples due to the excessive PbI_2 in the precursor solutions[16,18-19].

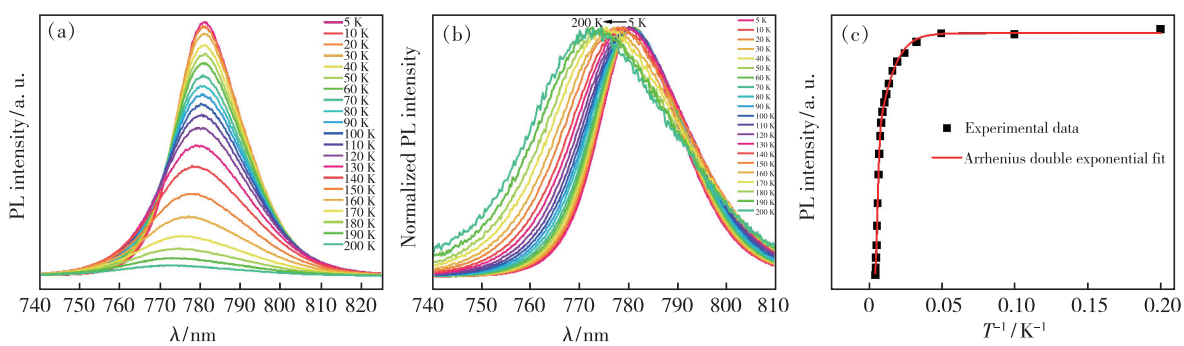

Fig. 2 (a) Temperature-dependent photoluminescence spectra of as-fabricated film. (b) Normalized photoluminescence spectra of (a). (c) Rrelationship between photoluminescence intensity and reciprocal of temperature.

The exciton-phonon interaction is examined by measuring the photoluminescence spectra in the temperature vary of T = 5 ~ 200 K as proven in Fig. 2(a) and (b). Fig. 2(a) and (b) show the temperature-dependent unnormalized and normalized photoluminescence spectra of the $Cs_{0.05}FA_{0.79}MA_{0.16}PbI_{2.52}$-

$Br_{0.48}$ perovskite thin film. In addition, a 9.36 nm blueshift of photoluminescence peak position from 781.07 nm to 771.71 nm is observed, and accompanied by a slight broadening of FWHM from 19.4 nm to 34.32 nm. The blueshift reflects the lattice deformation potential and exciton-phonon coupling[20], and it is related to the photoluminescence emission of bound excitons on the short wavelength side. For the pure $FAPbI_3$ or $MAPbI_3$, the phase transition temperature is about at 120 K. Here the Cs and Br doping may change the crystal structure[21]. It may be the reason of the absence of phase transition phenomenon.

Fig. 2(c) shows the relationship between photoluminescence intensity and reciprocal of temperature, which can be fitted by the Arrhenius equation[22]:

$$I(T) = \frac{I_0}{1 + C_1\exp\left(-\frac{E_1}{k_B T}\right) + C_2\exp\left(-\frac{E_2}{k_B T}\right)}, \quad (1)$$

where $I(T)$ and $I(0)$ are the emission intensity at the temperatures T and 0 K, C_1 and C_2 are the relative weight of the two quenching processes, k_B is Boltzmann constant, E_1 and E_2 are the activation energies related with the nonradiative recombination process. E_1 and E_2 obtained by fitting are 123.45 meV and 10.73 meV respectively. The high E_1 is considered as the potential barrier between the localized potential minima and the non-radioactive recombination centers, and the low E_2 might be attributed localized exciton binding energy[23-25].

The Bose-Einstein double oscillator model only considers the relative contributions of acoustic phonon and optical phonon, but does not consider the sum of all possible phonon in Brillouin zone, and depends on the fact that the electron-phonon contribution symbols given by the two oscillators are opposite[26]. The model is used to analyze the bandgap change, and described as follows[27]:

$$E_0(T,M) = E_0 + \frac{A_{ac}}{M_{ac}\omega_{ac}}\left(\frac{1}{e^{\omega_{ac}/kT} - 1} + \frac{1}{2}\right) + \frac{A_{opt}}{M_{opt}\omega_{opt}}\left(\frac{1}{e^{\omega_{opt}/kT} - 1} + \frac{1}{2}\right), \quad (2)$$

where E_0 is non-renormalized bandgap energy, A_{ac} and A_{opt} represent the relative weight of oscillators (or the electron-phonon coupling coefficients), ω_{ac} and ω_{opt} are the acoustic and optical phonon energies, and M_{ac} and M_{opt} are the relative atomic masses of the oscillator.

Fig. 3 (a) shows the temperature-dependent bandgap of the $Cs_{0.05}FA_{0.79}MA_{0.16}PbI_{2.52}Br_{0.48}$ perovskite thin film. The model provides an excellent fit (red solid line) to the experimental data obtained for the film across the temperature range studied. The best fitting parameters were obtained as E_0 = 1.639 eV, A_{ac} = 3.485, A_{opt} = −12.99, ω_{ac} = 50.65 meV and ω_{opt} = 285.42 meV. The non-renormalized bandgap E_0 is reasonable, and it is thought between 1.62 eV and 1.65 eV[15,28-29]. As shown in Fig. 3 (a), the bandgap of $Cs_{0.05}FA_{0.79}MA_{0.16}PbI_{2.52}Br_{0.48}$ increases non-linearly with the temperature, and the contribution of optical phonon and acoustic phonon to bandgap obeys the Bose-Einstein distribution.

The total photoluminescence emission broadening can be described by the sum of three broadening contributions given by the Segall expression as follows[30]:

$$\Gamma(T) = \Gamma_{inh} + \Gamma_{AC} + \Gamma_{LO}, \quad (3)$$

$$\Gamma(T) = \Gamma_{inh} + \varphi_{AC}T + \frac{\varphi_{LO}}{e^{(E_{LO}/kT)} - 1}, \quad (4)$$

where Γ_{inh} is the non-uniform expansion constant caused by exciton-exciton interaction and crystal disorder, which is independent of temperature. In the second term (Γ_{AC}), φ_{AC} represents the phonon coupling coefficient of exciton-phonon interaction, which is mainly related to the temperature-dependent deformation potential interaction. The third term (Γ_{LO}), φ_{LO} is the exciton-longitudinal optical phonon coupling coefficient or Fröhlich coupling coefficient, which is related to the Bose-Einstein distribution of LO phonons given as $1/(e^{(E_{LO}/kT)} - 1)$[26]. Here, E_{LO} is the energy of the LO phonons, k is the Boltzmann constant.

Fig. 3(b) shows the temperature-dependent FWHM of the $Cs_{0.05}FA_{0.79}MA_{0.16}PbI_{2.52}Br_{0.48}$ perovskite thin film. The contribution to broadening from acoustic phonon and LO phonon is also plotted. The FHWM

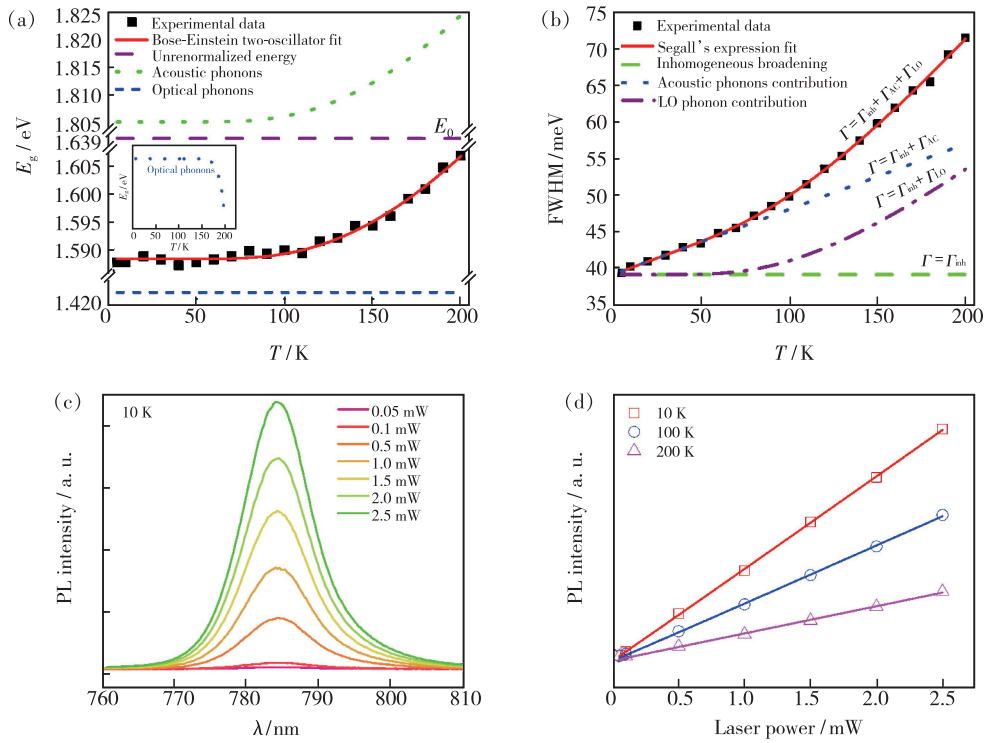

Fig. 3 (a) Temperature-dependent photoluminescence bandgap of $Cs_{0.05}FA_{0.79}MA_{0.16}PbI_{2.52}Br_{0.48}$ perovskite thin film. The experimental data (black squares) are fitted using a Bose-Einstein two-oscillator model (red solid line). At the same time, the relative contributions of non-renormalized bandgap energy (horizontal purple dashed line) and lead-like phonon (green dotted line) and X-like optical phonon (blue dotted line) to energy drift are given. (b) Temperature-dependent FWHM for $Cs_{0.05}FA_{0.79}MA_{0.16}PbI_{2.52}Br_{0.48}$ perovskite thin film. The black squares are the experimental data fitted using Segall expression (red solid line). The temperature-dependent the photoluminescence exciton linewidth broadening arising from acoustic phonon interplay $\Gamma(T) = \Gamma_{inh} + \Gamma_{AC}$ (blue dash-dot line), LO phonon interplay $\Gamma(T) = \Gamma_{inh} + \Gamma_{LO}$ (purple dash-dot line), inhomogeneous broadening term $\Gamma(T) = \Gamma_{inh}$ (horizontal green dotted line). (c) Photoluminescence spectra evolution with the laser power at 10 K. (d) Relationship between photoluminescence intensity and incident laser power at 10, 100, 200 K.

broadening by the contribution of acoustic phonon increases linearly with the temperature, while LO phonon is on the contrary. It indicates the strong exciton-phonon interactions in $Cs_{0.05}FA_{0.79}MA_{0.16}PbI_{2.52}Br_{0.48}$ perovskite thin film. The best fitted parameters by equation (4) are $\Gamma_{inh} = 39.19$ meV, $\varphi_{AC} = 88.93$ μeV · K^{-1}, $\varphi_{LO} = 81.67$ meV and $E_{LO} = 32.77$ meV.

With the increase of laser power at 10 K, there is no blueshift or redshift in photoluminescence spectra as shown in Fig. 3(c). Fig. 3(d) shows the relationship between excitation power and photoluminescence intensity at 10, 100, 200 K. The photoluminescence intensity I exponentially increasing with excitation power P could be expressed as

$$I \propto P^{\gamma}, \tag{5}$$

here the parameter γ can reflect the carrier recombination processes physically. If $\gamma = 1$, it indicates that the radiation recombination is dominant[31]. If $1 < \gamma < 2$, the photoluminescence is mainly from exciton-like recombination, and if $\gamma < 1$, the photoluminescence might be from free-to-bound and donor-acceptor pairs recombination[4]. Here the fitted γ are 1.006 3 and 1.013 2 at 10 K and 100 K, respectively, which means the photoluminescence is from exciton recombination. While the fitted γ = 0.998 6 at 200 K indicates the radiation recombination is mainly from free-to-bound and donor-acceptor pairs, which means the defect associated photoluminescence arises at high temperature[31].

4 Conclusion

In this paper, the temperature-dependent photoluminescence properties of $Cs_{0.05}FA_{0.79}MA_{0.16}PbI_{2.52}$-

$Br_{0.48}$ perovskite thin film treated with chlorobenzene were studied. The temperature-dependent photoluminescence reveals the effect of exciton-phonon coupling. With the increase of temperature, the photoluminescence shows blue-shift and bi-exponential quenching. The activation energies E_1 and E_2 fitted by Arrhenius equation are 123.45 meV and 10.73 meV respectively. The bandgap fitted by the Bose-Einstein double harmonic oscillator model gives the non-renormalized bandgap energy 1.639 eV, and the non-uniform expansion and exciton-phonon coupling coefficients of the photoluminescence were obtained by Segall expression fitting. At 10 K and 100 K, the photoluminescence of $Cs_{0.05}FA_{0.79}MA_{0.16}PbI_{2.52}Br_{0.48}$ is dominated by the exciton recombination, while at 200 K, the photoluminescence is donated by free-to-bound and donor-acceptor pairs, which indicates that the photoluminescence related to defects is produced at high temperature.

Response Letter is available for this paper at: http://cjl.lightpublishing.cn/thesisDetails#10.37188/CJL.20210195.

References:

[1] DAI J, ZHENG H G, ZHU C, *et al.* Comparative investigation on temperature-dependent photoluminescence of $CH_3NH_3PbBr_3$ and $CH(NH_2)_2PbBr_3$ microstructures [J]. *J. Mater. Chem.* C, 2016, 4(20): 4408-4413.

[2] ZHOU H P, CHEN Q, LI G, *et al.* Interface engineering of highly efficient perovskite solar cells [J]. *Science*, 2014, 345(6196): 542-546.

[3] ZHANG C R, DUAN J J, QIN F F, *et al.* $CsPbBr_3$ interconnected microwire structure: temperature-related photoluminescence properties and its lasing action [J]. *J. Mater. Chem.* C, 2019, 7(34): 10454-10459.

[4] SUN L W, WANG R, WANG W, *et al.* Excitonic optical properties of cesium trifluoroacetate induced $CsPbBr_3$ thin film with anti-solvent treatment [J]. *Opt. Mater.*, 2020, 106: 110005-1-7.

[5] CHEN Y H, TAN S Q, LI N X, *et al.* Self-elimination of intrinsic defects improves the low-temperature performance of perovskite photovoltaics [J]. *Joule*, 2020, 4(9): 1961-1976.

[6] BING J M, HUANG S J, HO-BAILLIE A W Y. A review on halide perovskite film formation by sequential solution processing for solar cell applications [J]. *Energy Technol.*, 2020, 8(4): 1901114-1-22.

[7] LIU Y, CHEN P A, HU Y Y. Recent developments in fabrication and performance of metal halide perovskite field-effect transistors [J]. *J. Mater. Chem.* C, 2020, 8(47): 16691-16715.

[8] DUAN J L, XU H Z, SHA W E I, *et al.* Inorganic perovskite solar cells: an emerging member of the photovoltaic community [J]. *J. Mater. Chem.* A, 2019, 7(37): 21036-21068.

[9] SHI L, BUCKNALL M P, YOUNG T L, *et al.* Gas chromatography-mass spectrometry analyses of encapsulated stable perovskite solar cells [J]. *Science*, 2020, 368(6497): eaba2412-1-7.

[10] KOGO A, CHIKAMATSU M. Cesium iodide post-treatment of organic-inorganic perovskite crystals to improve photovoltaic performance and thermal stability [J]. *Nanoscale*, 2020, 12(42): 21605-21609.

[11] SUN D L, ZHANG C, KAVAND M, *et al.* Spintronics of organometal trihalide perovskites [EB/OL]. (2016-08-02). http://arxiv.org/abs/1608.00993.

[12] WU K W, BERA A, MA C, *et al.* Temperature-dependent excitonic photoluminescence of hybrid organometal halide perovskite films [J]. *Phys. Chem. Chem. Phys.*, 2014, 16(41): 22476-22481.

[13] WEHRENFENNIG C, LIU M Z, SNAITH H J, *et al.* Charge carrier recombination channels in the low-temperature phase of organic-inorganic lead halide perovskite thin films [J]. *APL Mater.*, 2014, 2(8): 081513-1-10.

[14] KIM Y C, JEON N J, NOH J H, *et al.* Beneficial effects of PbI_2 incorporated in organo-lead halide perovskite solar cells [J]. *Adv. Energy Mater.*, 2016, 6(4): 1502104-1-8.

[15] JACOBSSON T J, CORREA-BAENA J P, ANARAKI E H, *et al.* Unreacted PbI_2 as a double-edged sword for enhancing the performance of perovskite solar cells [J]. *J. Am. Chem. Soc.*, 2016, 138(32): 10331-10343.

[16] CHEN P, BAI Y, WANG S C, *et al.* *In situ* growth of 2D perovskite capping layer for stable and efficient perovskite solar cells [J]. *Adv. Funct. Mater.*, 2018, 28(17): 1706923-1-10.

[17] BI D Q, GAO P, SCOPELLITI R, *et al.* High-performance perovskite solar cells with enhanced environmental stability based on amphiphile-modified $CH_3NH_3PbI_3$ [J]. *Adv. Mater.*, 2016, 28(15): 2910-2915.

[18] KOH T M, SHANMUGAM V, GUO X T, *et al.* Enhancing moisture tolerance in efficient hybrid 3D/2D perovskite photovoltaics [J]. *J. Mater. Chem.* A, 2018, 6(5): 2122-2128.

[19] CHO K T, ZHANG Y, ORLANDI S, *et al.* Water-repellent low-dimensional fluorous perovskite as interfacial coating for 20% efficient solar cells [J]. *Nano Lett.*, 2018, 18(9): 5467-5474.

[20] JING P T, ZHENG J J, IKEZAWA M, *et al.* Temperature-dependent photoluminescence of CdSe-core CdS/CdZnS/ZnS-multishell quantum dots [J]. *J. Phys. Chem.* C, 2009, 113(31): 13545-13550.

[21] ZHOU W K, CHEN S L, ZHAO Y C, *et al.* Constructing $CsPbBr_3$ cluster passivated-triple cation perovskite for highly efficient and operationally stable solar cells [J]. *Adv. Funct. Mater.*, 2019, 29(14): 1809180-1-11.

[22] BIMBERG D, SONDERGELD M, GROBE E. Thermal dissociation of excitons bounds to neutral acceptors in high-purity GaAs [J]. *Phys. Rev.* B, 1971, 4(10): 3451-3455.

[23] ZHENG X H, CHEN H, YAN Z B, *et al.* Influence of the deposition time of barrier layers on optical and structural properties of high-efficiency green-light-emitting InGaN/GaN multiple quantum wells [J]. *J. Appl. Phys.*, 2004, 96(4): 1899-1903.

[24] HWANG J S, GOKARNA A, CHO Y H, *et al.* Direct comparison of optical characteristics of InGaN-based laser diode structures grown on pendeo epitaxial GaN and sapphire substrates [J]. *Appl. Phys. Lett.*, 2007, 90(13): 131908-1-3.

[25] LIU L, WANG L, LI D, *et al.* Influence of indium composition in the prestrained InGaN interlayer on the strain relaxation of InGaN/GaN multiple quantum wells in laser diode structures [J]. *J. Appl. Phys.*, 2011, 109(7): 073106-1-5.

[26] SARAN R, HEUER-JUNGEMANN A, KANARAS A G, *et al.* Giant bandgap renormalization and exciton-phonon scattering in perovskite nanocrystals [J]. *Adv. Opt. Mater.*, 2017, 5(17): 1700231.

[27] GÖBEL A, RUF T, CARDONA M, *et al.* Effects of the isotopic composition on the fundamental gap of CuCl [J]. *Phys. Rev.* B, 1998, 57(24): 15183-15190.

[28] FONDELL M, JACOBSSON T J, BOMAN M, *et al.* Optical quantum confinement in low dimensional hematite [J]. *J. Mater. Chem.* A, 2014, 2(10): 3352-3363.

[29] JACOBSSON T J, EDVINSSON T. Quantum confined Stark effects in ZnO quantum dots investigated with photoelectrochemical methods [J]. *J. Phys. Chem.* C, 2014, 118(22): 12061-12072.

[30] RUDIN S, REINECKE T L, SEGALL B. Temperature-dependent exciton linewidths in semiconductors [J]. *Phys. Rev.* B, 1990, 42(17): 11218-11231.

[31] WANG H N, JI Z W, QU S, *et al.* Influence of excitation power and temperature on photoluminescence in InGaN/GaN multiple quantum wells [J]. *Opt. Express*, 2012, 20(4): 3932-3940.

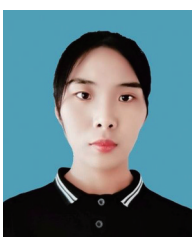

张琼(1998 –),女,云南宣威人,硕士研究生,2021 年于江苏科技大学获得学士学位,主要从事半导体发光材料及钙钛矿太阳能电池的研究。

E-mail: 18362885213@163.com

戴俊(1981 –),男,江苏扬州人,博士,教授,博士研究生导师,2012 年于东南大学获得博士学位,主要从事半导体发光材料及器件的研究。

E-mail: daijun@just.edu.cn